NeuroImage: Clinical 22 (2019) 101687

Contents lists available at ScienceDirect

NeuroImage: Clinical

journal homepage: www.elsevier.com/locate/ynicl

Resting state network modularity along the prodromal late onset Alzheimer's disease continuum

Joey A. Contreras[a,b,c,e], Andrea Avena-Koenigsberger[f], Shannon L. Risacher[a,b], John D. West[a,b], Eileen Tallman[a,b], Brenna C. McDonald[a,b,e,g], Martin R. Farlow[b,g], Liana G. Apostolova[a,b,e,g], Joaquín Goñi[a,b,h], Mario Dzemidzic[a,b,e,g], Yu-Chien Wu[a,b], Daniel Kessler[i], Lucas Jeub[c,d], Santo Fortunato[c,d], Andrew J. Saykin[a,b,c,e,g,*], Olaf Sporns[a,b,c,d,e,f,*]

[a] Department of Radiology and Imaging Sciences, Indiana University School of Medicine (IUSM), Indianapolis, IN, USA
[b] Indiana Alzheimer Disease Center, IUSM, Indianapolis, IN, USA
[c] Indiana University Network Science Institute, Bloomington, IN, USA
[d] School of Informatics, Computing and Engineering, Indiana University, Bloomington, IN, USA
[e] Program in Medical Neuroscience, Paul and Carole Stark Neurosciences Research Institute, Indiana University School of Medicine, Indianapolis, IN, USA
[f] Department of Psychological and Brain Sciences, Indiana University, Bloomington, IN, USA
[g] Department of Neurology, IUSM, Indianapolis, IN, USA
[h] College of Engineering, Purdue University, West Lafayette, IN, USA
[i] Departments of Statistics and Psychiatry, University of Michigan, Ann Arbor, MI, USA

ARTICLE INFO

Keywords:
Alzheimer's disease
Resting state
Brain networks
Functional connectivity
Connectomics

ABSTRACT

Alzheimer's disease is considered a disconnection syndrome, motivating the use of brain network measures to detect changes in whole-brain resting state functional connectivity (FC). We investigated changes in FC within and among resting state networks (RSN) across four different stages in the Alzheimer's disease continuum. FC changes were examined in two independent cohorts of individuals (84 and 58 individuals, respectively) each comprising control, subjective cognitive decline, mild cognitive impairment and Alzheimer's dementia groups. For each participant, FC was computed as a matrix of Pearson correlations between pairs of time series from 278 gray matter brain regions. We determined significant differences in FC modular organization with two distinct approaches, network contingency analysis and multiresolution consensus clustering. Network contingency analysis identified RSN sub-blocks that differed significantly across clinical groups. Multiresolution consensus clustering identified differences in the stability of modules across multiple spatial scales. Significant modules were further tested for statistical association with memory and executive function cognitive domain scores. Across both analytic approaches and in both participant cohorts, the findings converged on a pattern of FC that varied systematically with diagnosis within the frontoparietal network (FP) and between the FP network and default mode network (DMN). Disturbances of modular organization were manifest as greater internal coherence of the FP network and stronger coupling between FP and DMN, resulting in less segregation of these two networks. Our findings suggest that the pattern of interactions within and between specific RSNs offers new insight into the functional disruption that occurs across the Alzheimer's disease spectrum.

1. Introduction

For some time, Alzheimer's disease (AD) has been considered a disconnection syndrome (Delbeuck et al., 2003; Geschwind, 1965), and for this reason, graph theory-based whole-brain network analysis may offer a powerful way of understanding the abnormal dynamic interactions and connectivity patterns of distributed brain regions. Specifically, the use of network approaches to analyze resting state functional MRI (rs-fMRI) data may help provide new measures to quantify differences between groups and characterize how the brain's functional architecture changes in the context of AD. Network modules, generally defined as clusters of network nodes that are more densely connected within each cluster and less densely connected between clusters (Newman and Girvan, 2004), are ubiquitous in complex networks (Fortunato, 2010). Modules are also a characteristic hallmark of brain connectivity (Sporns and Betzel, 2016) and may play important roles in

* Corresponding authors at: Department of Radiology and Imaging Sciences, Indiana University School of Medicine (IUSM), Indianapolis, IN, USA.
E-mail addresses: asaykin@iupui.edu (A.J. Saykin), osporns@indiana.edu (O. Sporns).

https://doi.org/10.1016/j.nicl.2019.101687
Received 17 August 2018; Received in revised form 12 December 2018; Accepted 20 January 2019
Available online 22 January 2019

the functioning of large-scale brain networks (Sporns, 2013; Petersen and Sporns, 2015; Betzel et al., 2017).

In the human brain, modules derived from resting state fMRI are commonly called “resting state networks” (RSNs), and are defined as groups of brain regions that exhibit internally coherent fluctuations of resting state blood oxygenation level dependent (BOLD) responses (Greicius et al., 2003; Fox et al., 2005). This modular organization of functional connectivity (FC) represents stable sub-systems or “building blocks” that support, singly or through mutual interactions, different domains of cognition and behavior (Petersen and Sporns, 2015; Cohen and D'Esposito, 2016; Wig, 2017). Long-term changes in modules are observed in development (Alexander-Bloch et al., 2010), across the human lifespan (Betzel et al., 2014; Chan et al., 2014) and aging (Meunier et al., 2009a; Gallen et al., 2016; Schlesinger et al., 2017), and exhibit characteristic patterns associated with age-related neurodegenerative diseases (Gottlich et al., 2013). Recent methodological advances include the consideration of multiscale organization that is increasingly recognized as a hallmark of modular brain networks (Meunier et al., 2009b; Betzel and Bassett, 2017).

Resting state networks and modules exhibit specific patterns of disruption in AD (Contreras et al., 2015; Damoiseaux et al., 2012; Rombouts et al., 2005). Specifically, brain regions that make up the default mode network (DMN), which are highly functionally connected among healthy older adults, lose their “connectedness” in cases such as dementia (Greicius et al., 2004; Sorg et al., 2007; Rombouts et al., 2005; Zhu et al., 2013). Similarly, FC in AD patients exhibits a significant reduction of clustering, both involving brain regions that are affected in AD (e.g., the hippocampus) and on an overall global scale (Supekar et al., 2008), implying a re-organization of functional modules. Other studies have also reported reduced long-distance FC (Sanz-Arigita et al., 2010) and a weakening between connections that link modules, with the latter effect linked to cognitive dysfunction (de Haan et al., 2012).

Likewise, better performance among cognitive tasks has been correlated with highly functionally connected brain regions comprising the executive network. Among those with MCI and dementia, these canonical RSNs do not exhibit the same functional connectivity patterns (i.e., high connectivity among brain regions belonging to a particular RSN) (Weiler et al., 2014). Additionally, multiple studies show that interaction between the DMN and executive networks is critical for complex cognitive tasks and that their relationship serves as an important marker for cognitive health (Fox et al., 2005; Spreng et al., 2010; Vincent et al., 2008; Boord et al., 2017; Crittenden et al., 2016). This is particularly relevant in the case of AD, because the DMN may serve as an important diagnostic biomarker for AD due to evidence that brain atrophy, amyloid-β plaque, tau deposition, and metabolic deficits co-occur in the DMN (Buckner et al., 2009; Mohan et al., 2016; Wang et al., 2013).

While numerous studies have examined FC and RSN dysfunction in AD, robust signatures of disease-related changes in the organization of functional networks at multiple scales have remained elusive. To comprehensively examine how FC networks are disrupted in the course of AD we embarked on a strategy that: (1) uses a combination of two distinct analysis approaches, probing for specific RSN deficits as well as disturbances of multiscale organization; (2) examines functional connectivity differences between different clinical stages leading up to AD, including subjective cognitive decline (SCD) and mild cognitive impairment (MCI) populations; and (3) demonstrates replicability across two independently acquired cohorts on two 3 T MRI platforms. Specifically, we used a two-pronged network analysis strategy. First, we analyzed differences in within- and between-RSN functional connectivity using block-wise network contingency analysis carried out on a standard RSN partition. Second, we applied a multi-scale community detection approach that allowed us to identify functional connectivity modules across multiple spatial scales. The combination of these two approaches allowed us to pinpoint network components and interactions that differed between participants grouped by clinical status. To test the reproducibility of our findings we conducted a second set of analyses on a diagnostically and demographically comparable, but otherwise completely independent replication cohort. Our study reveals new insights into the gradual disruption of specific aspects of RSN architecture and modular organization along the prodromal AD spectrum.

2. Methods

2.1. Participants

The Indiana University Institutional Review Board approved the study, and written informed consent was obtained from each participant from both cohorts. The first cohort included a subset of older adults from the Indiana Alzheimer's disease Center (IADC), hereafter referred to as the IADC cohort. Participants were included based on availability of rs-fMRI data: 31 cognitively normal controls (CN group, psychometrically normal with no significant cognitive concerns), 27 participants with significant cognitive concerns despite cognitive test performance within the normal range (SCD group), 14 participants with amnestic mild cognitive impairment (MCI group), and 12 AD patients (AD group). The replication cohort consisted of a non-overlapping group of participants enrolled in the Indiana Memory and Aging Study, herein referred to as the IMAS cohort: 13 in the CN group, 16 in the SCD group, 21 with amnestic MCI, and 8 AD patients (AD group). Data from this second group were included in a prior publication addressing a different approach (Contreras et al., 2017). One-way ANOVA was used to test for differences in age, sex, education, and neurocognitive variables between groups. Chi-squared tests were used to assess differences across cohorts in sex and diagnosis group membership. Demographic information for both the IADC and IMAS cohorts is presented in Table 1.

2.2. Neurocognitive variables

All participants underwent a comprehensive clinical assessment and neuropsychological battery as part of the Uniform Dataset 2.0 or 3.0 (Weintraub et al., 2009, 2018). Data from the IADC cohort included: 1) an executive function composite score, which was an average of the z-scores (calculated relative to a non-overlapping cognitively normal control group) from the following tasks: Trail Making Part B seconds to complete (Partington and Leiter, 1949), Digit Span Forward, and Digit Span Backward (Wechsler, 1987, 1997; 2) an episodic memory composite score which was an average of the z-scores from the following tasks: Logical Memory (immediate, delayed), Craft Stories (immediate, delayed) (Weintraub et al., 2018), and Rey Auditory Verbal Learning Test (RAVLT, immediate, delayed) (Schmidt, 1996).

The IMAS cohort data included: 1) an executive function composite score, which was an average of the z-scores from the following tasks: Wisconsin Card Sorting Test (WCST) (categories correct and perseverative errors) (Heaton et al., 1993), Test of Practical Judgement (TOP-J; a measure evaluating judgment related to safety, medical, social/ethical and financial issues; Rabin et al., 2007), Trail Making Test A seconds to complete, Trail Making Test B seconds to complete (Partington and Leiter, 1949), Digit Span Forward, and Digit Span Backward (Wechsler, 1987, 1997); and 2) an episodic memory composite score, which was an average of the task scores from the California Verbal Learning Test (CVLT-II; total, short, and long delay) (Delis et al., 1987, 2000), and Craft Stories (immediate, delayed) (Craft et al., 1996; Weintraub et al., 2018).

2.3. Image acquisition and preprocessing

Participants from the IADC cohort were imaged on a 3 T Siemens Prisma MRI scanner with a 64-channel receiver-only head coil. Whole

Table 1
Participant demographics and cognitive scores in IADC and IMAS cohort. Values for age, education, executive function and episodic memory are the means and standard deviations within each group.

IADC demographics					
	CN	SCD	MCI	AD	Stats
N	31	27	14	12	–
Age (yrs; mean, s.d.)	66.97 (6.12)	70.11 (9.92)	69.00 (9.54)	69.83 (13.63)	NS*
Sex (M/F)	8/23	9/18	8/6	6/6	NS†
Education (yrs; mean, s.d.)	16.55 (2.35)	17.11 (2.36)	16.21 (2.15)	14.67 (3.55)	NS*
Executive Function (mean, s.d.)	0.10 (0.63) §≠	−0.07 (0.58) §≠	−0.98 (1.28) ǂ¥≠	−3.96 (2.90) ǂ¥§	$p < .05$*
Episodic Memory (mean, s.d.)	0.37 (0.68) ¥§≠	−0.13 (0.80) ǂ§≠	−1.50 (0.86) ǂ¥≠	−2.50 (0.83) ǂ¥§	$p < .05$*
IMAS demographics					
N	13	16	21	8	–
Age (yrs; mean, s.d.)	67.15 (5.51)	73.38 (7.95)	73.33 (8.98)	76.38 (8.98)	NS*
Sex (M/F)	1/12	8/8	8/13	2/6	NS†
Education (yrs; mean, s.d.)	17.31 (1.93)	17.37 (1.93)	16.00 (2.28)	16.13 (3.76)	NS*
Executive Function (mean, s.d.)	−0.12 (0.71) ≠	0.33 (0.54) §≠	−0.54 (1.14) ¥≠	−3.49 (2.42) ǂ¥§	$p < .05$*
Episodic Memory (mean, s.d.)	0.30 (0.64) §≠	0.07 (0.77) §≠	−2.00 (0.73) ǂ¥≠	−4.60 (1.15) ǂ¥§	$p < .05$*

Group differences are assessed with *one-way ANOVA and †Chi-squared tests. Post-hoc *t*-tests (2-sample, 2-sided), $p < .05$ (uncorrected) applied to cognitive scores: ǂ significantly different from CN, ¥ significantly different from SCD, § significantly different from MCI, ≠ significantly different from AD.

brain rs-fMRI data were collected in participants who were instructed to think of nothing in particular and to remain still with eyes closed. We employed a multi-band sequence as detailed in Xu et al. (2013): gradient-echo echo-planar imaging (GE-EPI), scan duration 10 min 7 s, 500 blood oxygenation level dependent (BOLD) contrast sensitive volumes, multi-band acceleration factor of 3, repetition/echo time TR/TE = 1200 ms/29 ms, 2.5 × 2.5 × 2.5 mm^3 voxels, and 54 interleaved axial slices. The IMAS cohort was imaged on a 3 T Siemens Tim Trio MRI scanner with a 12-channel receiver-only head coil using a GE-EPI sequence, scan duration 6 min 9 s, 161 BOLD contrast sensitive volumes, repetition/echo time TR/TE = 2250 ms/29 ms, 2.5 × 2.5 × 3.5 mm^3 voxels, 39 interleaved axial slices covering the whole brain, GRAPPA acceleration factor 2, and 3-dimensional prospective acquisition correction (PACE) for head motion (Thesen et al., 2000).

Participants from both cohorts had an anatomical MRI with whole brain coverage using a 3D Magnetization Prepared Rapid Gradient Echo (MPRAGE) sequence (220 sagittal slices, 1.1 × 1.1 × 1.2mm^3 voxels) per the Alzheimer's Disease Neuroimaging Initiative (ADNI-1 and ADNI-2) imaging protocol. In the IADC cohort, we implemented an accelerated protocol (GRAPPA, $R = 2$) to reduce imaging time from 9:14 s (IMAS dataset) to 5:12 s. Two short (12 s) spin echo echo planar imaging (SE-EPI) scans (TR/TE = 1560/49.8 ms, one in A-P and one in P-A phase direction) with an imaging volume and voxel size identical to the rs-fMRI GE-EPI were acquired immediately before the resting state scan for field mapping. These phase-reversed SE-EPI scans provide a field map for correcting EPI geometric distortion (Smith et al., 2004). This procedure was performed using FSL's topup/applytopup (Smith et al., 2004), which yielded improved signal localization across the whole brain, with the most notable improvements in frontal and temporal areas.

The resulting unwarped rs-fMRI data were preprocessed within the Matlab framework using FSL as recommended by Power et al. (2012, 2014): 1) slice time correction; 2) motion correction; 3) tissue segmentation of white matter (WM), gray matter (GM), and CSF using T1-weighted MPRAGE; 4) co-registration of T1-weighted MPRAGE to rs-fMRI volumes through a sequence of transformations (FSL's FLIRT 6 DOFs, FLIRT 12 DOFs and nonlinear FNIRT); 5) application of brain parcellation with 278 regions of interest (ROI) (Shen et al., 2013) in native rs-fMRI space (this parcellation derived from a large resting state dataset includes ROIs that have similar size and are neither too fine nor too coarse); 6) use of mode 1000 normalization and linear detrending of the BOLD signal; 7) inclusion of 18 regressors (6 head motion parameters, mean WM, CSF, and whole-brain tissue-based signals and their 9 derivatives) and a scrubbing procedure to exclude extreme head motion outlier volumes (method adapted from Power et al., 2014); 8) application of a first-order Butterworth bandpass filter (0.009 Hz to 0.08 Hz); and 9) use of 5 principal components in the WM and CSF tissue BOLD signal to regress them from the GM signal. These processed rs-fMRI data were then used to quantify the functional connectivity of brain regions in each participant by computing correlation coefficients (Pearson's *r*) between mean BOLD time series of each ROI pair, which were compiled into a 278 × 278 functional connectivity matrix. Brain regions were further ordered into nine blocks: seven well-defined cortical RSNs (Yeo et al., 2011), plus blocks of subcortical and cerebellar regions. Details can be found in Contreras et al. (2017). All network analyses in this paper were carried out on Fisher z-transformed FC estimates.

2.4. Functional connectivity analysis: block-wise comparison

To determine whether functional connectivity patterns differed significantly between clinical groups, we pursued an approach similar to that previously described as network contingency analysis (Sripada et al., 2014). The approach performs a block-wise comparison of functional connections within and between specific RSNs (blocks) to determine if these connections differ significantly between groups of participants. The method uses a nonparametric permutation test to determine significant differences and avoids testing for large numbers of single edges by instead comparing edge counts obtained from FC sub-blocks. The analysis proceeded along the following steps. First, functional connectivity differences between the control and AD clinical groups were expressed as a t-statistic. Second, group affiliations were randomly permuted 10,000 times and t-statistics were computed from these permuted samples to build an empirical null distribution. Third, the whole-brain FC matrix was subdivided into 9 × 9 sub-blocks corresponding to seven canonical RSNs (Yeo et al., 2011) plus cerebellum and subcortex, as described above. Fourth, we counted, for each of the 45 unique sub-blocks (9 diagonal and (9*8)/2 off-diagonal), the number of t-values exceeding a t-threshold (t_{thr}), testing for both $t > t_{thr}$ and $t < -t_{thr}$. We varied t_{thr} between $t = 2.0$ and $t = 6.0$, in steps of 0.25, to ensure robustness. Fifth, we repeated steps three and four for each of the 10,000 random permutations, thus generating a distribution for the number of functional connections differing between groups under the statistical criterion set by the t-threshold. Finally, we computed exact *p*-values based on the comparison of FC counts in empirical versus permuted samples in each unique FC sub-block and applied a Bonferroni correction. The analysis was first carried out comparing CN

and AD subjects in the IADC cohort, and then performed on CN and AD participants in the IMAS cohort. In the replication cohort, we focused only on FC sub-blocks that showed significant Bonferroni-corrected differences between CN and AD participants in the IADC cohort.

Network contingency analysis can capture group differences in the number of individual edges that significantly differ within each block. To also test for differences in FC magnitude for each FC sub-block across clinical groups, we computed the median functional connectivity within each of the 45 unique FC sub-blocks for each individual participant. Median FC values were computed for all individuals in both cohorts and used for subsequent group-wise comparisons as well as brain-behavior regression analysis.

2.5. Functional connectivity analysis: multiscale modularity

To determine significant differences in the network community structure (modularity) of FC patterns across clinical groups, we performed modularity maximization using a fast variant of the Louvain algorithm (Blondel et al., 2008). A novel aspect of our analysis is the adoption of a method probing for modularity at multiple spatial scales or resolutions, followed by the creation of a consensus across scales. This technique, called multiresolution consensus clustering (Jeub et al., 2018), was adapted for use with correlation matrices by implementing a suitable null model in the modularity function. Briefly, the analysis proceeds along the following steps. First, using the Louvain modularity maximization algorithm, partitions were sampled from a wide range of the resolution parameter that tunes the objective function to different spatial scales. The range of the resolution parameter was selected such that the full set of samples ranged from a minimal setting (where the number of modules is equal to 1) to a maximal setting (where the number of modules is equal to the number of nodes). For each FC matrix, 10,000 sample partitions were collected within this range, employing an event sampling strategy to ensure approximately equal coverage of all scales present in the network. Second, the ensemble of sample partitions was combined into a co-classification (CC) matrix that summarized, for each pair of nodes, the proportion of all partitions for which the node pair was co-assigned to the same module. This proportion can maximally range between zero (no co-classification at any resolution) and one (perfect co-classification across all resolutions). Third, the full multiresolution ensemble of partitions was subjected to a divisive hierarchical clustering algorithm based on assessing significance of pairwise co-classification of nodes. This step delivers a tree (dendrogram) of nested partitions, taken to represent the multiscale modular structure of the network.

Multiresolution consensus clustering was carried out on FC matrices averaged for each diagnostic group, as well as on individual FC matrices. To test for differences involving specific RSNs the co-classification matrix was analyzed within the same 9×9 sub-blocks used previously for FC analysis. Focusing on those significant sub-blocks that survived Bonferroni correction in FC network contingency analysis across both primary and replication data sets (see above), we tested if these sub-blocks also exhibited differences (across participant groups) in the frequency with which their constituent node pairs were co-classified into the same modules. This was assessed by computing the median block-wise co-classification for all individuals in both cohorts. These data were later used for group-wise comparisons as well as brain-behavior regression analyses.

Finally, we examined differences in modular organization across participant groups by placing the nine canonical RSNs within data-driven multiresolution consensus partitions derived from averaged FC matrices for each group. Projecting the nine canonical RSNs into each group's consensus partition allowed visualization of how these canonical RSNs mapped onto the group-specific multiscale consensus.

2.6. Linear regression analysis and brain-behavior relationship

Using individual FC data, the median FC and CC magnitudes for the sub-blocks that survived network contingency analysis in both primary and replication data sets (see above) were regressed against two behavioral scores, for executive function and memory (both converted to z-scores corrected for age, sex and education). FC magnitude and CC magnitude were computed as the median FC and median CC within each sub-block, corrected for effects of age, sex and education, and converted to neural z-scores. The relation between neural and behavioral scores was computed as a Spearman rank-order correlation. To assess statistical significance, in addition to associated p-values, we computed neural-behavioral Spearman correlations for 10,000 random permutations of participant's behavioral scores against un-permuted neural scores, thus forming an empirical null distribution of correlation values against which the experimental correlation values could be compared.

2.7. Data availability

Detailed clinical data cannot be made publicly available for confidentiality reasons. However, qualified researchers may apply for access to de-identified data, contingent on any required Institutional Review Board approvals, data security assurances, a signed data use agreement, and approval by the study principal investigator. Analysis tools for detecting network communities and for multiresolution consensus clustering are available at https://github.com/GenLouvain/GenLouvain/commits/master and at https://github.com/LJeub/HierarchicalConsensus, respectively. Other network analysis tools are at https://sites.google.com/site/bctnet/. Force embedded network layouts were performed using http://mrvar.fdv.uni-lj.si/pajek/.

3. Results

3.1. Participant cohorts

Participant characteristics and cognitive scores for both cohorts are presented in Table 1. No significant differences were found in age, sex, or education between groups across cohorts. Significant group membership differences were found across cohorts. The IADC cohort had proportionally more CN and less MCI participants compared to the IMAS cohort.

Comparison of cognitive scores across groups revealed the following significant differences (listed here in only one direction): 1) IADC, executive function: between CN and MCI, AD; between SCD and MCI, AD; and between MCI and AD; 2) IADC, episodic memory: between CN and SCD, MCI, AD; between SCD and MCI, AD; between MCI and AD; 3) IMAS, executive function: between CN and AD; between SCD and MCI, AD; between MCI and AD; 4) IMAS, episodic memory: between CN and MCI, AD; between SCD and MCI, AD; between MCI and AD. See Table 1 for details.

3.2. Functional connectivity

Averaged FC patterns for the four participant groups are presented in Fig. 1, with node orders in the FC matrices arranged by RSN sub-block. FC matrices averaged by RSN sub-blocks are shown for both IADC and IMAS cohorts to demonstrate cross-cohort reproducibility. Block-wise network contingency analysis was applied to compare functional connections within and between a priori RSNs and to determine which RSN blocks differed significantly between diagnostic groups. In the IADC cohort, at a t-threshold of 3.5, five sub-blocks survived statistical testing (Bonferroni corrected, $p < .05/45$). Two sub-blocks showed decreased FC in the AD group compared to the CN

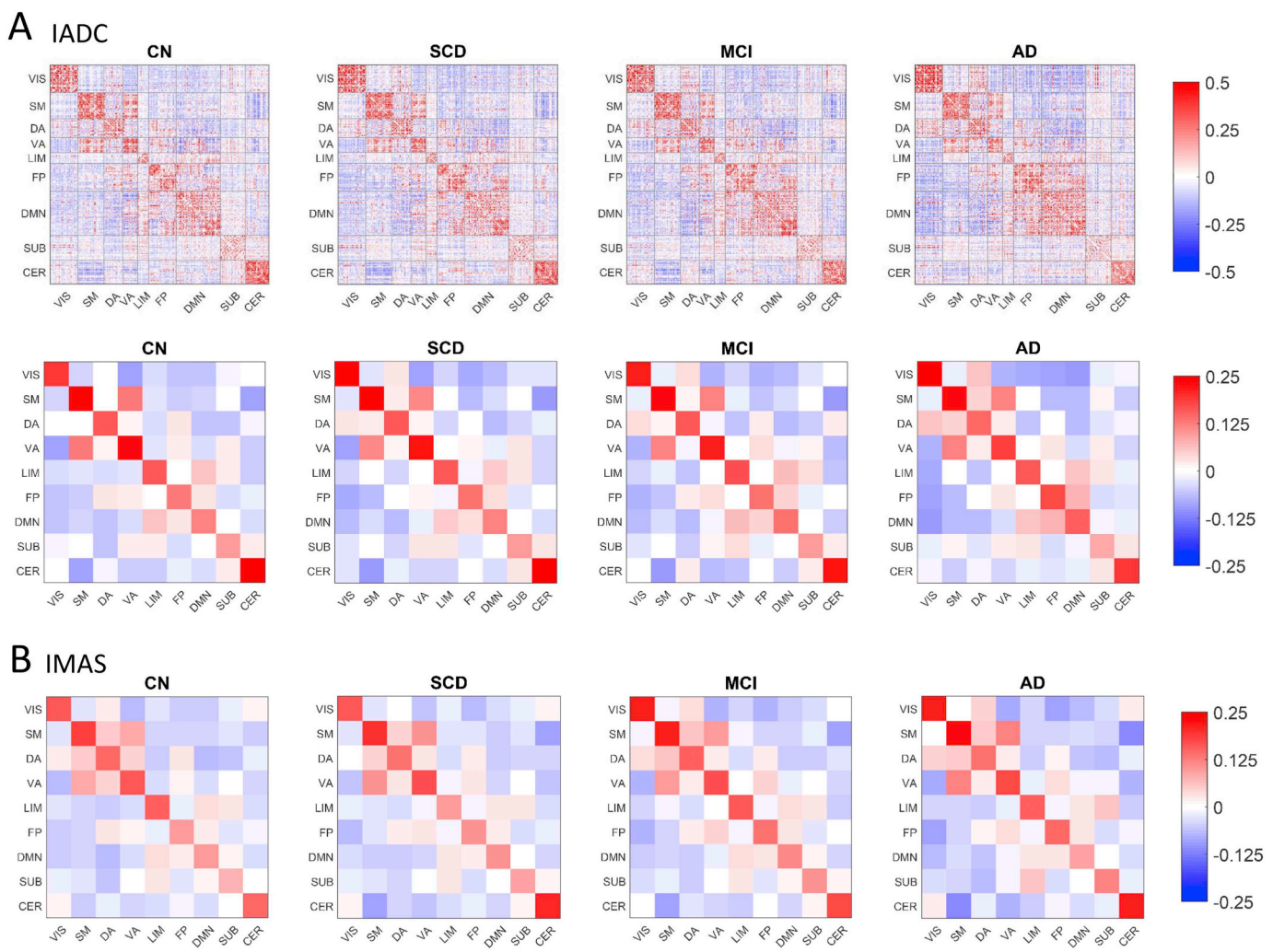

Fig. 1. Averaged FC matrices by diagnosis for both cohorts. A) IADC cohort. The top row shows the connectivity of all brain region pairs using a 278 × 278 parcellation (Shen et al., 2013). Each participant's matrix was quantified using z-transformed Pearson correlation coefficients between mean BOLD time series of each ROI pair and averaged across participants within each diagnostic group. Bottom row shows brain regions further ordered into nine blocks: seven well-defined cortical RSNs (Yeo et al., 2011), plus blocks of subcortical and cerebellar regions resulting in 9 × 9 FC matrices (VIS-visual network, SM-somatomotor network, DA-dorsal attention network, VA-ventral attention network, LIM-limbic network, FP-frontoparietal network, DMN-default mode network, SUB-subcortical brain regions, CER-cerebellar brain regions). B) IMAS cohort, showing group-averaged connectivity RSN matrices separated by diagnosis.

group: the somatomotor (SM) network, and the DMN-VIS (visual network) interaction. Three sub-blocks showed increased FC in the AD group compared to the CN group: the FP network, and the interactions DMN-FP and DA-VIS. Of these five sub-blocks, only two also showed significant differences in subsequent statistical testing in the IMAS cohort (Bonferroni corrected, $p < .05/5$): the FP block, corresponding to the fronto-parietal network, and the FP-DMN interaction block, corresponding to the block linking the fronto-parietal and the default mode network. The FP and FP-DMN group differences passed Bonferroni correction across broad ranges of t-values (FP: t = [2.0, 3.5] and t = [2.0, 3.75]; FP-DMN: t = [2.0, 5.5] and t = [2.75, 4.25]; IADC and IMAS cohorts, respectively). All subsequent analyses were carried out exclusively on the FP and FP-DMN blocks.

To further test for significant FC differences within the FP and FP-DMN blocks, we computed the median FC for each of these blocks for all individual participants and tested for group differences. Test statistics were computed by performing permutation testing (10,000 permutations); reported *p*-values are uncorrected. Fig. 2 shows FC data for individual participants from the four participant groups in both cohorts. In the IADC cohort, significant differences were found between the CN and AD groups for both the FP ($p = .004$) and FP-DMN sub-blocks ($p = .0004$). In the IMAS cohort, significant differences were found only in the FP sub-block, both between CN and MCI groups ($p = .018$) and CN and AD groups ($p = .008$). No other comparisons reached significance.

3.3. Multiresolution consensus clustering

Co-classification (CC) matrices computed from the group-averaged FC (see Fig. 1) for the four participant groups are presented in Fig. 3, with node orders in the matrices arranged by RSN sub-block (matching the orderings shown in Fig. 1). CC matrices averaged by RSN sub-blocks are shown for both IADC and IMAS cohorts to demonstrate cross-cohort reproducibility. Focusing on the FP and FP-DMN sub-blocks identified in prior network contingency analysis, we tested whether the average co-classification for node-pairs within these two sub-blocks differed among individuals across groups, applying permutation testing (10,000 permutations); reported p-values are uncorrected. Fig. 4 shows the resulting group differences. In the IADC cohort, for the FP sub-block marginal differences were found between CN and MCI groups ($p = .051$) and significant differences were found between CN and AD groups ($p = .004$). For the FP-DMN sub-block, significant differences were found between the CN and AD groups ($p = .003$). All of these differences were replicated in the IMAS cohort (FP block CN/MCI

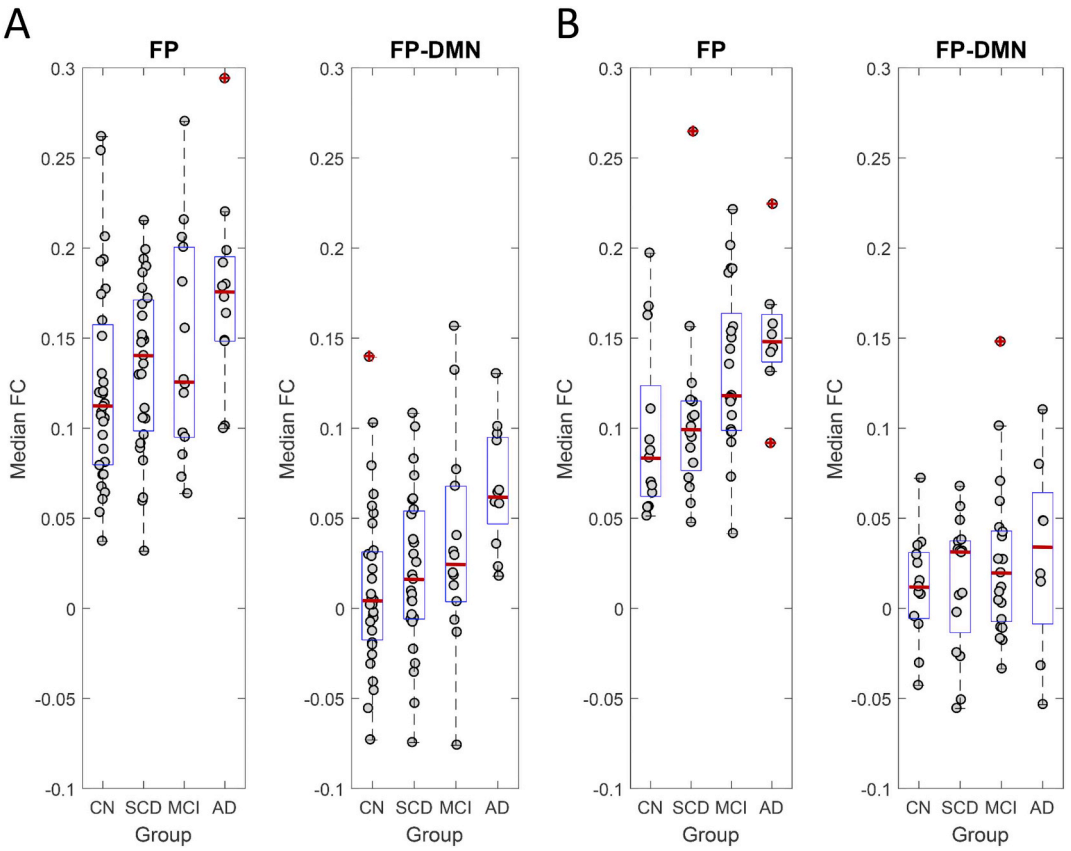

Fig. 2. Group-differences in median FC between diagnostic groups. Plots show A) IADC and B) IMAS cohorts, displaying median FC (per individual participant) for the FP and FP-DMN sub-blocks. Boxplots show median (red line), 25% and 75% percentiles (blue box) and outliers (red crosses). Significant group differences exist for AD (IADC FP, IADC FP-DMN, IMAS FP) as well as for MCI (IMAS FP), compared to CN groups. See text for details on statistical tests and *p*-values.

$p = .033$; FP block CN/AD $p = .015$; FP-DMN block CN/AD $p = .023$).

Differences in how canonical RSNs mapped onto each group's native modularity are visualized in Fig. 5. To generate this visualization, we first selected a cut in the multi-resolution hierarchy for which the number of modules across the four groups most closely matched the number of RSNs (nine) included in the study. We arranged the nodes for each clinical group according to this partition, and then overlaid the nine canonical RSNs onto these group-specific modules to determine how these RSNs are distributed within and across modules. Visualizing the overlay of the RSNs onto group partitions in the IADC cohort (Fig. 5A) further reveals differences in organizational structure between different clinical groups. Focusing on the FP and DMN, in the CN group the majority of brain regions (network nodes) constituting these two networks were organized into distinct and separate modules. In the AD group, this was no longer evident, as the majority of FP and DMN nodes were co-classified within the same module. This arrangement was also encountered in the IMAS cohort (Fig. 5B). In the IADC cohort, the loss in separation between FP and DMN was evident as early as the SCD group, but appears less clearly in the MCI group, indicating some nonlinearity in progression along the clinical spectrum.

Fig. 6 displays the overall organization of the group-averaged FC and CC patterns using the same node ordering as in Fig. 5, for the CN and AD groups in the IADC cohort. A major difference between the two groups is the smaller number of larger modules in the AD group compared to the CN group, which results in a less well separated (segregated) arrangement of the nine canonical RSNs. This is particularly evident when comparing the CC patterns across the two groups. Fig. 7 reinforces this point, displaying layouts for the CC patterns across the four groups in the IADC cohort. Node color indicates membership in the nine canonical RSNs. These CC layouts reveal that the largely intact segregation among RSNs in the CN group becomes progressively disturbed. Supporting our prior statistical analyses, this finding is particularly evident in the placement of FP and DMN nodes (blue and purple, respectively) which become increasingly intermingled with increasing severity along the clinical spectrum.

3.4. Regression analysis and brain-behavior relationship

Finally, we tested for significant correlations between candidate neural measures (median FC and median CC within the FP and the FP-DMN sub-blocks) and candidate behavioral measures (executive function and episodic memory), across all individual participants in both cohorts.

Across both cohorts and both neural measures (median block-wise FC and CC), brain-behavior relationships emerged most consistently when examining regressions of the FP sub-block data against the memory score (Fig. 8). In the IADC cohort, the median CC/episodic memory score regression reached significance (uncorrected Spearman's $\rho = -0.225$, $p = .046$) while the median FC/episodic memory score relationship was non-significant ($\rho = -0.073$, $p = .523$). In the IMAS cohort, both relationships reached significance ($\rho = -0.300$, $p = .024$ and $\rho = -0.360$, $p = .006$, respectively). Overall, these findings suggest that greater internal coherence (expressed as either increased FC or stronger CC) of the FP network is associated with lower episodic memory scores. No other brain-behavior regressions were reproducible across the two cohorts.

4. Discussion

There is general agreement that the brain of a patient with AD differs from that of a normally aging individual, especially in terms of its pattern of anatomical and functional inter-regional connections.

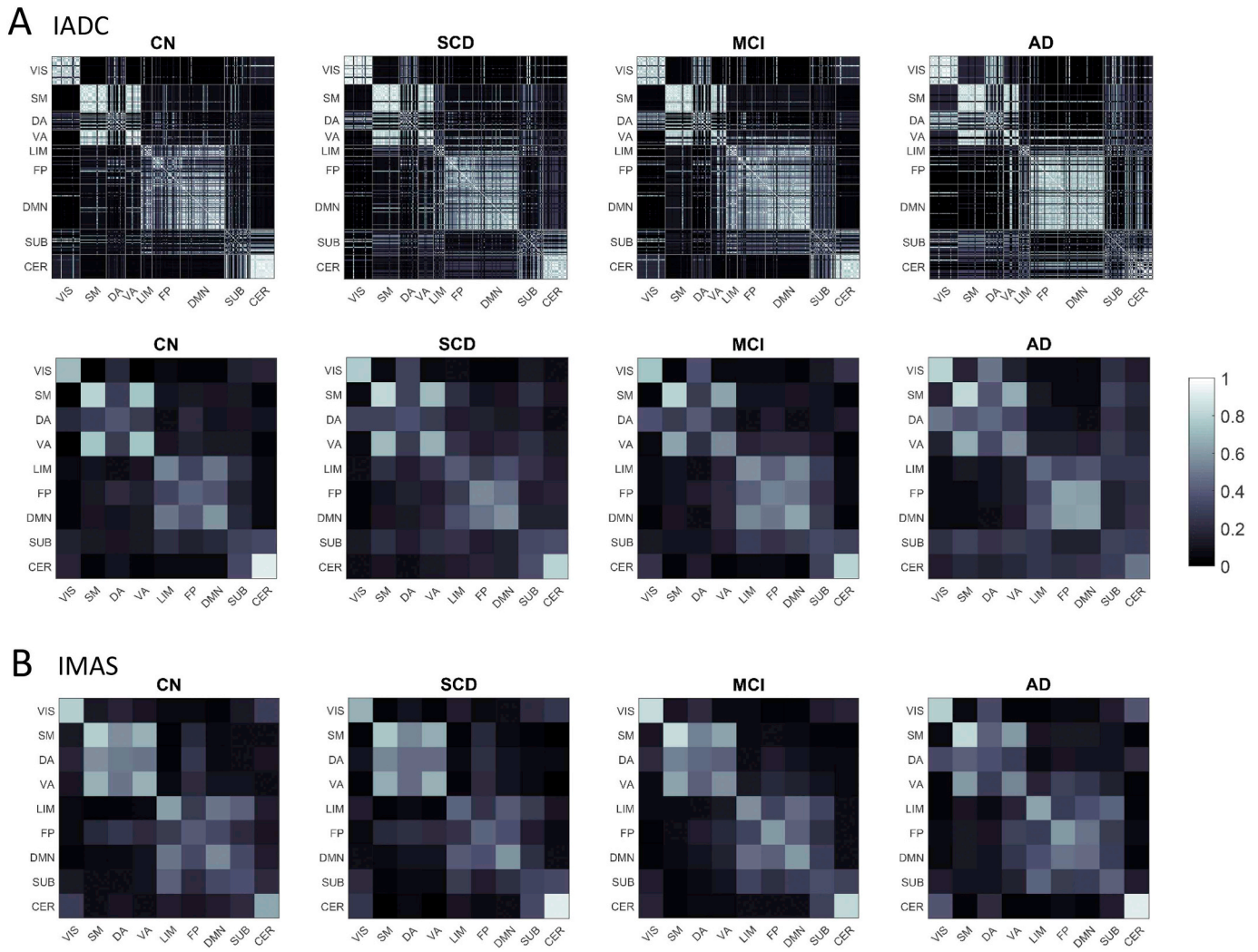

Fig. 3. Averaged CC matrices by diagnosis for both cohorts. A) IADC cohort. Top row shows unaveraged parcellation. Bottom row shows averaged values within the 9 RSN blocks B) IMAS cohort. CC matrices are displayed ranging between 0 (no co-classification) and 1 (perfect co-classification). Abbreviations of RSNs as in Fig. 1.

Often, studies focus solely on the connectivity alterations within individual networks. Such an approach, however, does not consider the complex interplay between regions from different brain systems and does not provide the integrative perspective needed to assess how the brain changes as disease progresses. In this study, we examined the modular organization of functional connectivity among multiple canonical RSNs within four separate participant groups along the AD spectrum, focusing on convergent results obtained with multiple analysis approaches that replicated across two independent participant cohorts. Our findings point to FC differences within and between the DMN and FP networks, with a pronounced tendency for the two networks to become less segregated and more intermingled in AD participants compared to controls. As mentioned earlier, the interaction between the DMN and FP network is highly correlated with the performance of complex cognitive tasks, indicating the importance of this relationship to cognitive health. We therefore put forth the idea that as disease severity worsens (i.e., from SCD to MCI to AD) these important functional connectivity patterns become less prominent or are no longer present (i.e., in AD). This decreased segregation between two critical networks implicated in AD (DMN and FP network) adds to the idea that AD is a disconnection syndrome. To reveal these changes in FC modular organization we relied on direct comparison of FC patterns within and between RSNs, as well as on a novel approach to characterize FC modules across multiple spatial scales.

Studies that have employed connectivity metrics have had initial successes in identifying AD biomarkers, with some reporting specific functional connectivity changes as the disease progresses. To date, multiple studies have reported RSN disturbances in patients with AD, MCI, presymptomatic autosomal dominant AD mutation carriers, and cognitively normal individuals carrying the *APOE* ε4 risk allele (Agosta et al., 2012; Badhwar et al., 2017; Dillen et al., 2017; Li et al., 2017; Lopez-Sanz et al., 2017; Nakamura et al., 2017; Schumacher et al., 2018). Our study expands upon these earlier reports by using a two-pronged network analysis strategy aiming to more fully characterize FC modular organization, and by testing the robustness of our findings across two independent cohorts of participants. Our findings consistently point to the FP and DMN networks, and their mutual interactions, as altered in participants with AD. While the FP intrinsic coherence appears to increase, so does the median functional connectivity between the FP and the DMN network, resulting in greater co-classification (i.e., reduced segregation). Some of these changes in FP/DMN organization are apparent at the earliest stages of AD, before cognitive symptoms manifest (e.g., Figs. 5 and 7).

The importance of the relationship between FP and DMN to cognition has long been hypothesized (Demertzi et al., 2013; Heine et al., 2012). For instance, internetwork coupling between these networks is believed to support cognitive processes such as decision-making, executive function and memory. In fact, age differences have been shown

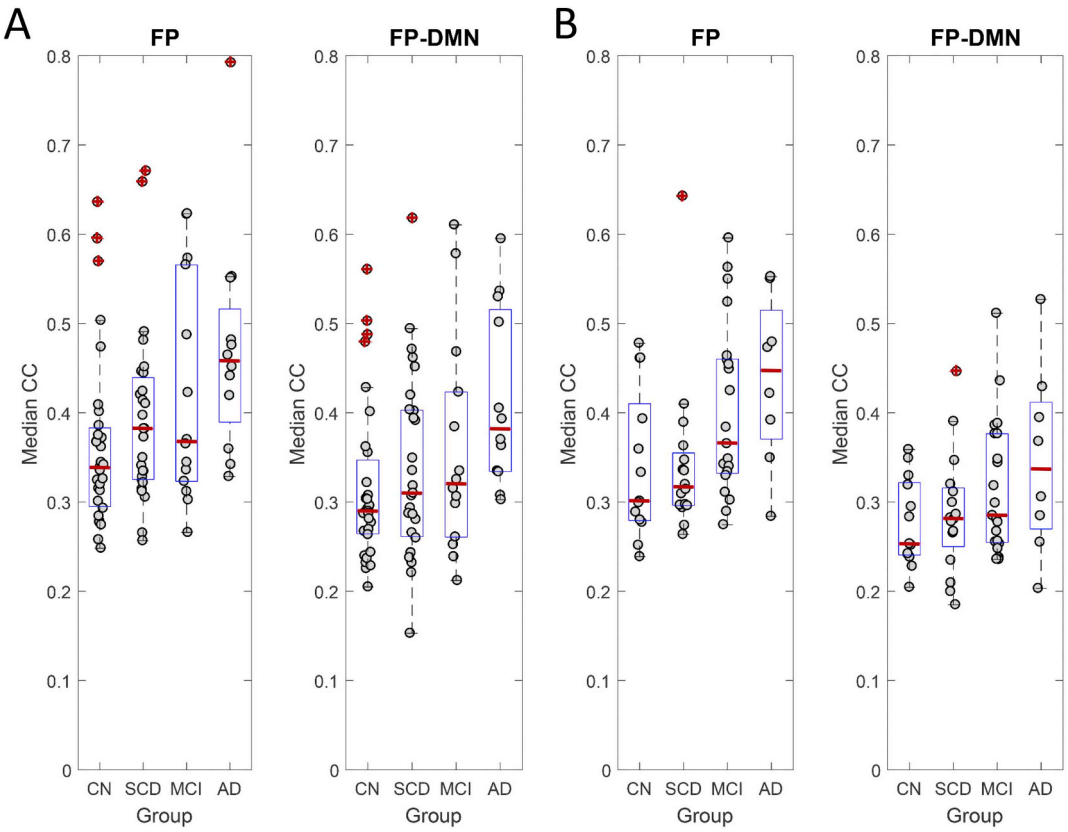

Fig. 4. Group-differences in median CC between diagnostic groups. Plots show A) IADC and B) IMAS cohorts, displaying median CC (per individual participant) for the FP and FP-DMN sub-blocks. Boxplots show median (red line), 25% and 75% percentiles (blue box) and outliers (red crosses). Significant group differences exist for AD (IADC FP, IADC FP-DMN, IMAS FP, IMAS FP-DMN) as well as for MCI (IADC FP, IMAS FP), compared to CN groups. See text for details on statistical tests and p-values.

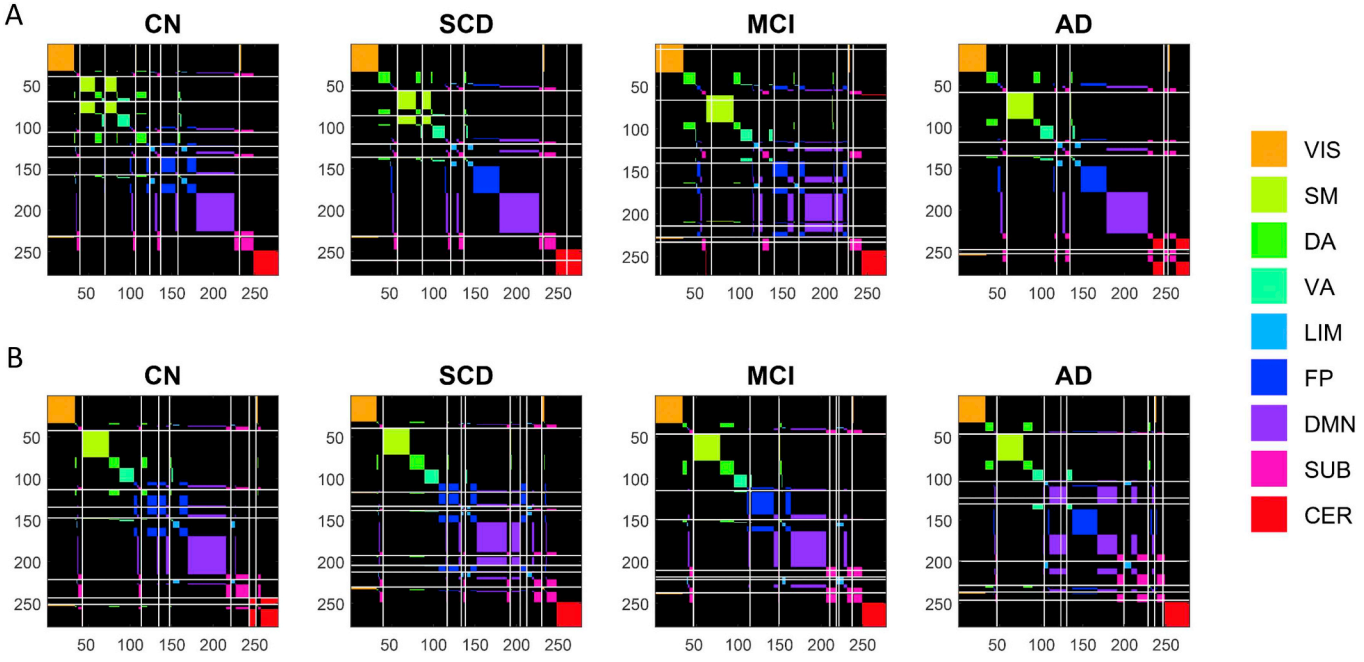

Fig. 5. Relation between group-specific modularity and canonical RSNs. Plots show A) IADC and B) IMAS cohorts, respectively. Diagnostic group consensus matrices show brain regions organized by their respective multi-scale modular partition (denoted via gray lines) which, for each group, most closely matched the number of RSNs included in this study (nine in total); note that this results in node orderings that differ between subject groups and cohorts. Superimposed is the canonical assignment of each node pair to a standard RSN (color code shown at right). As diagnosis becomes more severe the DMN (purple) and FP (blue) become less well separated within each group's sets of modules, and more intermingled (i.e. purple and blue modules are increasingly co-assigned to the same module).

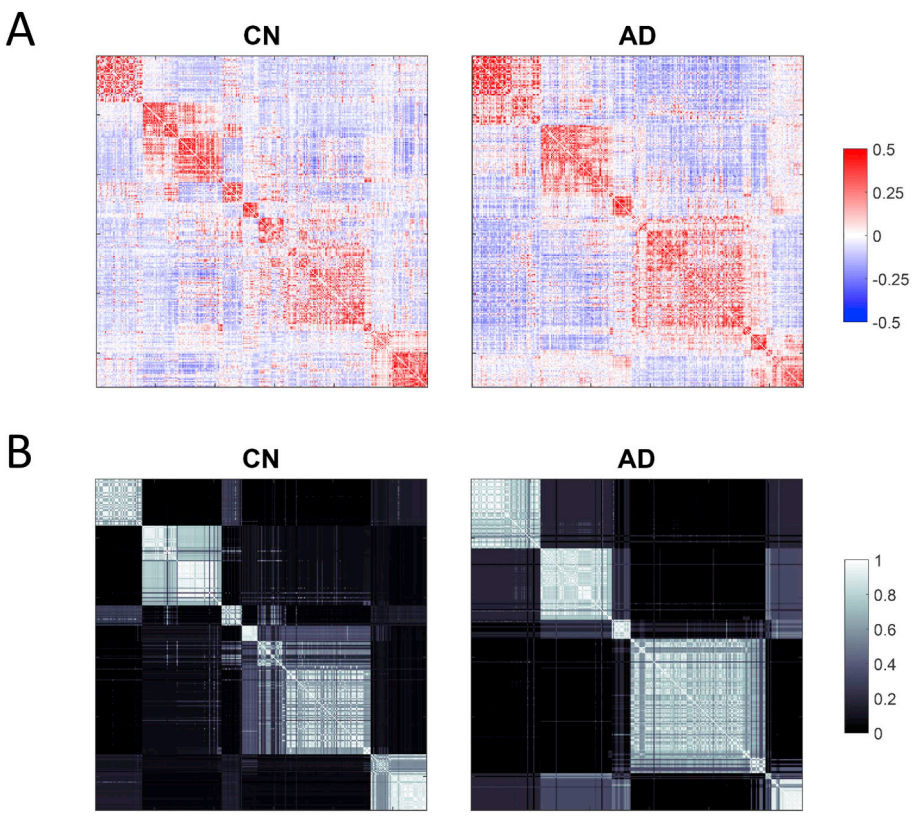

Fig. 6. Comparison of group-averaged FC and CC matrices. Plots show A) FC and B) CC matrices (IADC cohort), rearranged in each group's native partitioning scheme (as displayed in the corresponding panels in Fig. 5). Node orderings in the FC and CC panels for the CN group and the AD group correspond exactly, thus allowing direct comparison of the functional connectivity and co-classification patterns. Note the smaller number of internally coherent modules in the AD group, compared to the CN group, which is particularly apparent in the CC matrices (panels B).

in inter-network FC between DMN and FP, specifically demonstrating that between-network FC of the FP network can predict cognitive performance (Grady et al., 2016). How functional networks interact with each other in pathological conditions such as Alzheimer's disease is not well understood, however. Even less known is how this interaction, or lack thereof, manifests behaviorally. Therefore, our results

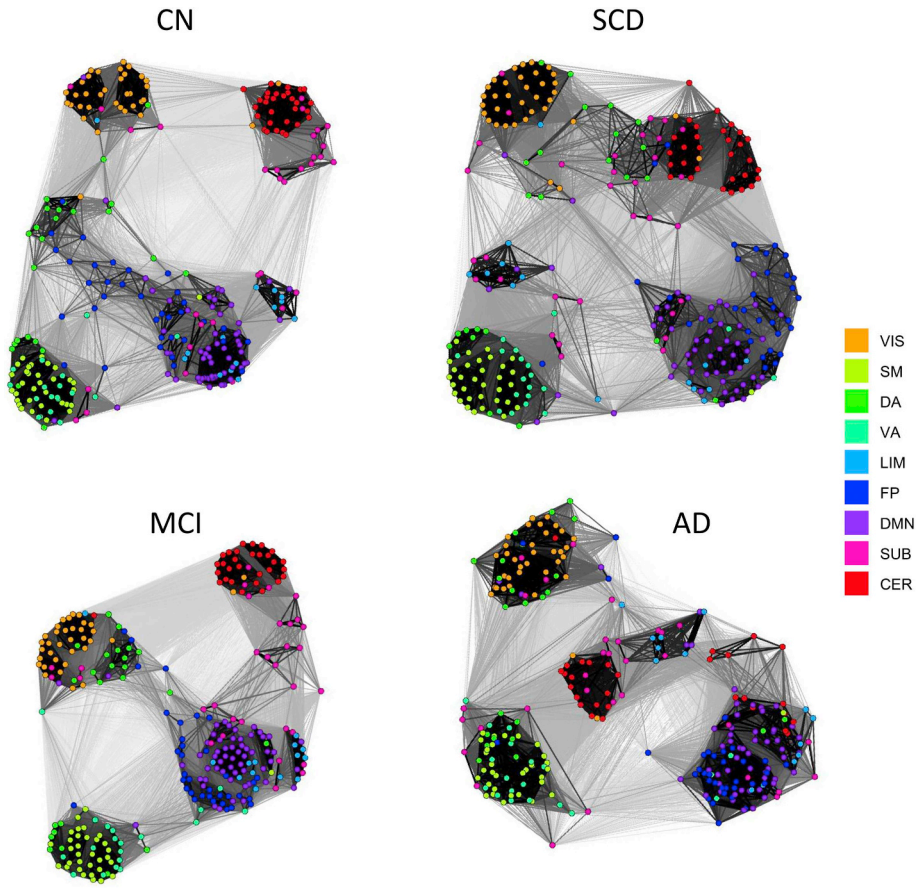

Fig. 7. Force-directed network visualizations of CC matrices (IADC cohort). Node positions were derived using the Kamada-Kawai layout algorithm (Kamada and Kawai, 1989) that assigns spring-like forces to network edges and then places nodes such that the energy stored in the edges is minimized. Node color indicates RSN membership. Note the central position of the FP network (blue nodes) in the CN group which is gradually lost, with FP and DMN (purple nodes) becoming increasingly co-classified and co-mingled.

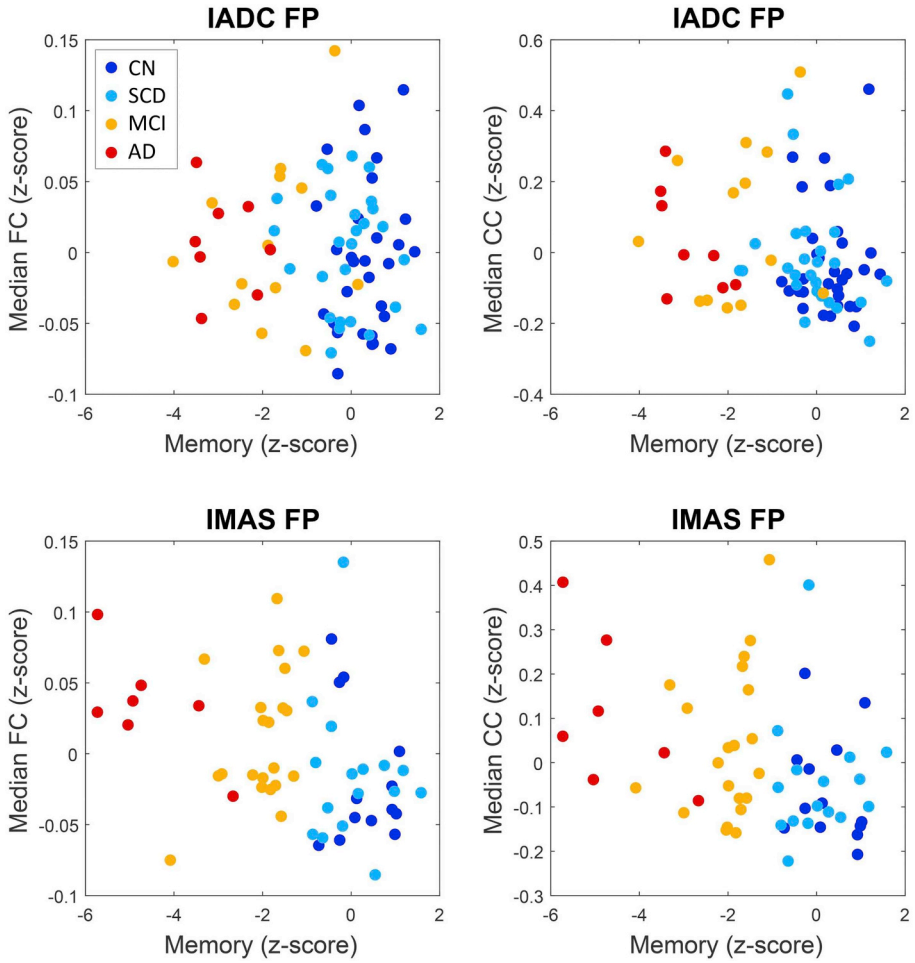

Fig. 8. Brain-behavior relationships. Panels show neural z-scores (median FC, median CC) and behavioral z-scores (memory score). Behavioral scores were missing for a small number of participants; these participants were excluded from this part of the analysis. Participants are color-coded by clinical group (CN, blue; SCD, light blue; MCI, yellow; AD, red). See main text for Spearman correlations and p-values.

demonstrating a significant difference in FC magnitude within FP and in the FP/DMN interaction between CN and AD groups may offer new insight into neural bases for specific cognitive dysfunctions. Our second (related) finding was showing that as the disease progressed, brain regions in the FP and DMN networks became less segregated and increasingly merged into one network module. Interestingly, other studies have shown that the frontoparietal network and default mode network engage in behaviorally relevant mutual interactions (Boly et al., 2009; Fox et al., 2005; Long et al., 2016). Specifically, it has been suggested that FP exerts control of the DMN by downregulating its activity (as the FP network becomes inhibited, the DMN becomes disinhibited) (Chen et al., 2013; Sridharan et al., 2008). These interactions are thought to mediate how the brain regulates higher-level cognitive processes (Buckner et al., 2008; Chen et al., 2013). This evidence would suggest that properly balanced interaction between the two networks is critical for healthy brain function and cognition. In fact, other studies have shown that disruptions in the dynamic interaction between networks is linked to attentional lapses and suboptimal performance in healthy individuals (Persson et al., 2007; Prado and Weissman, 2011; Weissman et al., 2006).

We add further evidence to the aforementioned critical relationship between DMN and FP networks by demonstrating that differences in modular organization of brain regions belonging to both RSNs is reflected in AD, a disease that greatly impairs cognition, memory, and sense of self. Furthermore, this breakdown of organization is partially evident in the MCI group (Figs. 2 and 4) and in cognitively normal patients with significant cognitive complaints (Fig. 5). This suggests that our network approach may have potential to help characterize complex diseases such as AD, and may guide further investigation into the functional connectivity and dynamic relationships between ROIs that are part of both RSNs, providing additional context for exploring disease spread.

An important feature of our study is the use of two parallel and distinct network analysis approaches to detect FC differences across clinical groups, as well as replication of main findings on a separate replication cohort. Network contingency analysis allows for the detection of block-wise differences in FC across groups of individuals (Sripada et al., 2014) while avoiding excessive multiple comparison testing (similar to the approach called network-based statistic; Zalesky et al., 2010). Multiresolution consensus clustering (Jeub et al., 2018) does not directly test for differences in FC, but instead generates a module co-classification matrix that records, for each pair of nodes, the propensity for these nodes to belong to the same module. The approach avoids the pitfalls of having to select a single scale (a single value of the resolution parameter in the modularity metric) for subsequent analysis, a step that requires setting statistical criteria that can be difficult to define or justify. The co-classification matrix naturally combines data from multiple scales, and thus provides a fuller picture of the stability and spatial organization of statistically significant FC modules. In combination, these two approaches complement each other as they employ different approaches for examining modular network structure.

There are limitations to the present study. Diagnostic group membership was significantly different across the two cohorts. Specifically, the IADC cohort had proportionally more CN and fewer MCI

participants compared to the IMAS cohort. The AD groups were also smaller than the other subgroups. The inclusion of additional participants to equalize sampling across groups could help to reproduce specific patterns between cohorts and could provide a broader range of neurocognitive scores across the samples. Second, while we analyzed the functional connectomes in both cohorts in the same manner, resting state scan duration and acquisition parameters (e.g., Siemens 3 T scanners and BOLD contrast sensitive sequence) differed. Mounting evidence suggests that longer rs-fMRI acquisition times can greatly improve data quality (Birn et al., 2013) as well as improve the stability and reproducibility of FC networks (Laumann et al., 2015). Our rs-fMRI acquisition in the more recent IADC cohort was superior, both spatially (smaller and isotropic voxels) and temporally (almost two-fold improvement in sampling rate), as well as from the scan duration perspective (10 min vs 6 min in the IMAS cohort). The legacy IMAS cohort also had slightly higher number of scrubbed BOLD volumes (mean of 10%). Despite these functional connectivity estimation limitations in the IMAS cohort, there was no bias across diagnostic groups. With these differences in mind, the replicability of results between cohorts supports the robustness of the main findings reported in our study.

Third, this study uses cross-sectional data; therefore, it is not certain that patients currently diagnosed as SCD or MCI will progress to AD. This shortcoming will be addressed with the ongoing collection of longitudinal data in the IADC cohort.

In summary, we have added further evidence that the dysregulation in modular organization in the FP network and between the DMN and FP network does carry clinical implications, specifically in the case of AD (Menon, 2011; Whitfield-Gabrieli and Ford, 2012). Thus, the combination of advanced neuroimaging techniques and network analysis may hold the potential to characterize pathological changes within AD, specifically by detecting incipient disturbances in brain functional systems.

Funding and acknowledgements

This study was supported, in part, by National Institute on Aging grants R01 AG019771, P30 AG10133, and K01 AG049050, and the Alzheimer's Association, Indiana Clinical and Translational Science Institute (UL1 TR001108), Indiana University-IU Health Strategic Research Initiative, and the IU Network Science Institute (IUNI). MRI scans were supported in part by the IU Department of Radiology and Imaging Sciences. DK was supported by NSF grant DMS-1646108. OS was also supported by NIH grant R01 AT009036-01. We thank Evgeny J. Chumin for valuable comments and discussion. We thank the staff of the Indiana Memory and Aging Study, the Indiana Alzheimer Disease Center, as well as the imaging staff of the Indiana Institute for Biomedical Imaging Sciences and the IU Center for Neuroimaging. We are very grateful to the study participants and their families who made this research possible.

References

Agosta, F., Pievani, M., Geroldi, C., Copetti, M., Frisoni, G.B., Filippi, M., 2012. Resting state fMRI in Alzheimer's disease: beyond the default mode network. Neurobiol. Aging 33, 1564–1578.
Alexander-Bloch, A.F., Gogtay, N., Meunier, D., Birn, R., Clasen, L., Lalonde, F., Lenroot, R., Giedd, J., Bullmore, E.T., 2010. Disrupted modularity and local connectivity of brain functional networks in childhood-onset schizophrenia. Front. Syst. Neurosci. 4, 147.
Badhwar, A., Tam, A., Dansereau, C., Orban, P., Hoffstaedter, F., Bellec, P., 2017. Resting-state network dysfunction in Alzheimer's disease: a systematic review and meta-analysis. Alzheimers Dement (Amst) 8, 73–85.
Betzel, R.F., Bassett, D.S., 2017. Multi-scale brain networks. NeuroImage 160, 73–83.
Betzel, R.F., Byrge, L., He, Y., Goñi, J., Zuo, X.N., Sporns, O., 2014. Changes in structural and functional connectivity among resting-state networks across the human lifespan. NeuroImage 102, 345–357.
Betzel, R.F., Medaglia, J.D., Papadopoulos, L., Baum, G.L., Gur, R., Gur, R., et al., 2017. The modular organization of human anatomical brain networks: accounting for the cost of wiring. Netw. Neurosci. 1, 42–68.
Birn, R.M., Molloy, E.K., Patriat, R., Parker, T., Meier, T.B., Kirk, G.R., et al., 2013. The effect of scan length on the reliability of resting-state fMRI connectivity estimates. NeuroImage 83, 550–558.
Blondel, V.D., Guillaume, J.L., Lambiotte, R., Lefebvre, E., 2008. Fast unfolding of communities in large networks. J. Stat. Mech. 10, P10008.
Boly, M., Tshibanda, L., Vanhaudenhuyse, A., Noirhomme, Q., Schnakers, C., Ledoux, D., et al., 2009. Functional connectivity in the default network during resting state is preserved in a vegetative but not in a brain dead patient. Hum. Brain Mapp. 30, 2393–2400.
Boord, P., Madhyastha, T.M., Askren, M.K., Grabowski, T.J., 2017. Executive attention networks show altered relationship with default mode network in PD. Neuroimage Clin. 13, 1–8.
Buckner, R.L., Andrews-Hanna, J.R., Schacter, D.L., 2008. The brain's default network: anatomy, function, and relevance to disease. Ann. N. Y. Acad. Sci. 1124, 1–38.
Buckner, R.L., Sepulcre, J., Talukdar, T., Krienen, F.M., Liu, H., Hedden, T., et al., 2009. Cortical hubs revealed by intrinsic functional connectivity: mapping, assessment of stability, and relation to Alzheimer's disease. J. Neurosci. 29, 1860–1873.
Chan, M.Y., Park, D.C., Savalia, N.K., Petersen, S.E., Wig, G.S., 2014. Decreased segregation of brain systems across the healthy adult lifespan. Proc. Nat. Acad. Sci. USA 111 (46), E4997–E5006.
Chen, A.C., Oathes, D.J., Chang, C., Bradley, T., Zhou, Z.W., Williams, L.M., et al., 2013. Causal interactions between fronto-parietal central executive and default-mode networks in humans. Proc. Natl. Acad. Sci. U. S. A. 110, 19944–19949.
Cohen, J.R., D'Esposito, M., 2016. The segregation and integration of distinct brain networks and their relationship to cognition. J. Neurosci. 36 (48), 12083–12094.
Contreras, J.A., Goni, J., Risacher, S.L., Sporns, O., Saykin, A.J., 2015. The structural and functional connectome and prediction of risk for cognitive impairment in older adults. Curr. Behav. Neurosci. Rep. 2, 234–245.
Contreras, J.A., Goni, J., Risacher, S.L., Amico, E., Yoder, K., Dzemidzic, M., et al., 2017. Cognitive complaints in older adults at risk for Alzheimer's disease are associated with altered resting-state networks. Alzheimers Dement (Amst) 6, 40–49.
Craft, S., Newcomer, J., Kanne, S., Dagogo-Jack, S., Cryer, P., Sheline, Y., Luby, J., Dagogo-Jack, A., Alderson, A., 1996 Jan-Feb. Memory improvement following induced hyperinsulinemia in Alzheimer's disease. Neurobiol. Aging 17 (1), 123–130.
Crittenden, B.M., Mitchell, D.J., Duncan, J., 2016. Task encoding across the multiple demand cortex is consistent with a frontoparietal and cingulo-opercular dual networks distinction. J. Neurosci. 36, 6147–6155.
Damoiseaux, J.S., Prater, K.E., Miller, B.L., Greicius, M.D., 2012. Functional connectivity tracks clinical deterioration in Alzheimer's disease. Neurobiol. Aging 33, e819–e830.
de Haan, W., van der Flier, W.M., Koene, T., Smits, L.L., Scheltens, P., Stam, C.J., 2012. Disrupted modular brain dynamics reflect cognitive dysfunction in Alzheimer's disease. NeuroImage 59, 3085–3093.
Delbeuck, X., Van der Linden, M., Collette, F., 2003. Alzheimer's disease as a disconnection syndrome? Neuropsychol. Rev. 13, 79–92.
Delis, D.C., Kramer, J.H., Kaplan, E., Ober, B.A., 1987. CVLT, California Verbal Learning Test: Adult Version: Manual. Psychological Corporation.
Delis, D., Kramer, J., Kaplan, E., Ober, B., 2000. California Verbal Learning Test, 2nd ed. The Psychological Corporation, San Antonio, TX Adult Version Manual.
Demertzi, A., Soddu, A., Laureys, S., 2013. Consciousness supporting networks. Curr. Opin. Neurobiol. 23, 239–244.
Dillen, K.N.H., Jacobs, H.I.L., Kukolja, J., Richter, N., von Reutern, B., Onur, O.A., et al., 2017. Functional disintegration of the default mode network in prodromal alzheimer's disease. J. Alzheimers Dis. 59, 169–187.
Fortunato, S., 2010. Community detection in graphs. Phys. Rep. 486 (3), 75–174.
Fox, M.D., Snyder, A.Z., Vincent, J.L., Corbetta, M., Van Essen, D.C., Raichle, M.E., 2005. The human brain is intrinsically organized into dynamic, anticorrelated functional networks. Proc. Natl. Acad. Sci. U. S. A. 102, 9673–9678.
Gallen, C.L., Turner, G.R., Adnan, A., D'Esposito, M., 2016. Reconfiguration of brain network architecture to support executive control in aging. Neurobiol. Aging 44, 42–52.
Geschwind, N., 1965. Disconnexion syndromes in animals and man. Brain 88, 237–294.
Gottlich, M., Munte, T.F., Heldmann, M., Kasten, M., Hagenah, J., Kramer, U.M., 2013. Altered resting state brain networks in Parkinson's disease. PLoS One 8, e77336.
Grady, C., Sarraf, S., Saverino, C., Campbell, K., 2016. Age differences in the functional interactions among the default, frontoparietal control, and dorsal attention networks. Neurobiol. Aging 41, 159–172.
Greicius, M.D., Krasnow, B., Reiss, A.L., Menon, V., 2003. Functional connectivity in the resting brain: a network analysis of the default mode hypothesis. Proc. Nat. Acad. Sci. USA 100 (1), 253–258.
Greicius, M.D., Srivastava, G., Reiss, A.L., Menon, V., 2004. Default-mode network activity distinguishes Alzheimer's disease from healthy aging: evidence from functional MRI. Proc. Nat. Acad. Sci. USA 101 (13), 4637–4642.
Heaton, R., Chelune, G., Talley, J., Kay, G., Curtis, G., 1993. Wisconsin card sorting test manual revised and expanded. Psychological assessment resources. (Odessa, FL).
Heine, L., Soddu, A., Gomez, F., Vanhaudenhuyse, A., Tshibanda, L., Thonnard, M., et al., 2012. Resting state networks and consciousness: alterations of multiple resting state network connectivity in physiological, pharmacological, and pathological consciousness States. Front. Psychol. 3, 295.
Jeub, L.G., Sporns, O., Fortunato, S., 2018. Multiresolution consensus clustering in networks. Sci. Rep. 8 (1), 3259.
Kamada, T., Kawai, S., 1989. An algorithm for drawing general undirected graphs. Inf. Process. Lett. 31 (1), 7–15.
Laumann, T.O., Gordon, E.M., Adeyemo, B., Snyder, A.Z., Joo, S.J., Chen, M.Y., et al., 2015. Functional system and areal organization of a highly sampled individual human brain. Neuron 87 (3), 657–670.
Li, Y., Yao, H., Lin, P., Zheng, L., Li, C., Zhou, B., et al., 2017. Frequency-dependent altered functional connections of default mode network in Alzheimer's disease. Front.

Aging Neurosci. 9, 259.
Long, J., Xie, Q., Ma, Q., Urbin, M.A., Liu, L., Weng, L., et al., 2016. Distinct interactions between fronto-parietal and default mode networks in impaired consciousness. Sci. Rep. 6, 38866.
Lopez-Sanz, D., Garces, P., Alvarez, B., Delgado-Losada, M.L., Lopez-Higes, R., Maestu, F., 2017. Network disruption in the preclinical stages of Alzheimer's disease: from subjective cognitive decline to mild cognitive impairment. Int. J. Neural Syst. 27, 1750041.
Menon, V., 2011. Large-scale brain networks and psychopathology: a unifying triple network model. Trends Cogn. Sci. 15, 483–506.
Meunier, D., Achard, S., Morcom, A., Bullmore, E., 2009a. Age-related changes in modular organization of human brain functional networks. NeuroImage 44 (3), 715–723.
Meunier, D., Lambiotte, R., Fornito, A., Ersche, K., Bullmore, E.T., 2009b. Hierarchical modularity in human brain functional networks. Front. Neuroinformatics 3, 37.
Mohan, A., Roberto, A.J., Mohan, A., Lorenzo, A., Jones, K., Carney, M.J., et al., 2016. The significance of the default mode network (DMN) in neurological and neuropsychiatric disorders: a review. Yale J. Biol. Med. 89, 49–57.
Nakamura, A., Cuesta, P., Kato, T., Arahata, Y., Iwata, K., Yamagishi, M., et al., 2017. Early functional network alterations in asymptomatic elders at risk for Alzheimer's disease. Sci. Rep. 7, 6517.
Newman, M.E., Girvan, M., 2004. Finding and evaluating community structure in networks. Phys. Rev. E Stat. Nonlinear Soft Matter Phys. 69, 026113.
Partington, J.E., Leiter, R.G., 1949. Partington's pathway test. Psychol. Serv. Cent. Bull. Vol. 1, 9–20.
Persson, J., Lustig, C., Nelson, J.K., Reuter-Lorenz, P.A., 2007. Age differences in deactivation: a link to cognitive control? J. Cogn. Neurosci. 19, 1021–1032.
Petersen, S.E., Sporns, O., 2015. Brain networks and cognitive architectures. Neuron 88 (1), 207–219.
Power, J.D., Barnes, K.A., Snyder, A.Z., Schlaggar, B.L., Petersen, S.E., 2012. Spurious but systematic correlations in functional connectivity MRI networks arise from subject motion. NeuroImage 59, 2142–2154.
Power, J.D., Mitra, A., Laumann TO, Snyder, A.Z., Schlaggar, B.L., Petersen, S.E., 2014. Methods to detect, characterize, and remove motion artifact in resting state fMRI. NeuroImage 84, 320–341.
Prado, J., Weissman, D.H., 2011. Heightened interactions between a key default-mode region and a key task-positive region are linked to suboptimal current performance but to enhanced future performance. NeuroImage 56, 2276–2282.
Rabin, L.A., Borgos, M.J., Saykin, A.J., Wishart, H.A., Crane, P.K., Nutter-Upham, K.E., et al., 2007. Judgment in older adults: development and psychometric evaluation of the Test of Practical Judgment (TOP-J). J. Clin. Exp. Neuropsychol. 29 (7), 752–767.
Rombouts, S.A., Barkhof, F., Goekoop, R., Stam, C.J., Scheltens, P., 2005. Altered resting state networks in mild cognitive impairment and mild Alzheimer's disease: an fMRI study. Hum. Brain Mapp. 26, 231–239.
Sanz-Arigita, E.J., Schoonheim, M.M., Damoiseaux, J.S., Rombouts, S.A., Maris, E., Barkhof, F., et al., 2010. Loss of 'small-world'networks in Alzheimer's disease: graph analysis of FMRI resting-state functional connectivity. PLoS One 5 (11), e13788.
Schlesinger, K.J., Turner, B.O., Lopez, B.A., Miller, M.B., Carlson, J.M., 2017. Age-dependent changes in task-based modular organization of the human brain. NeuroImage 146, 741–762.
Schmidt, M., 1996. Rey Auditory and Verbal Learning Test. A Handbook. Western Psychological Association, Los Angeles.
Schumacher, J., Peraza, L.R., Firbank, M., Thomas, A.J., Kaiser, M., Gallagher, P., et al., 2018. Functional connectivity in dementia with Lewy bodies: a within- and between-network analysis. Hum. Brain Mapp. 39, 1118–1129.
Shen, X., Tokoglu, F., Papademetris, X., Constable, R.T., 2013. Groupwise whole-brain parcellation from resting-state fMRI data for network node identification. NeuroImage 82, 403–415.
Smith, S.M., Jenkinson, M., Woolrich, M.W., Beckmann, C.F., Behrens, T.E., Johansen-Berg, H., 2004. Advances in functional and structural MR image analysis and implementation as FSL. NeuroImage 23 (Suppl. 1), S208–S219.
Sorg, C., Riedl, V., Mühlau, M., Calhoun, V.D., Eichele, T., Läer, L., Drzezga, A., Förstl, H., Kurz, A., Zimmer, C., Wohlschläger, A.M., 2007. Selective changes of resting-state networks in individuals at risk for Alzheimer's disease. Proc. Natl. Acad. Sci. 104 (47), 18760–18765.
Sporns, O., 2013. Making sense of brain network data. Nat. Methods 10 (6), 491.
Sporns, O., Betzel, R.F., 2016. Modular brain networks. Annu. Rev. Psychol. 67, 613–640.
Spreng, R.N., Stevens, W.D., Chamberlain, J.P., Gilmore, A.W., Schacter, D.L., 2010. Default network activity, coupled with the frontoparietal control network, supports goal-directed cognition. NeuroImage 53 (1), 303–317.
Sridharan, D., Levitin, D.J., Menon, V., 2008. A critical role for the right fronto-insular cortex in switching between central-executive and default-mode networks. Proc. Natl. Acad. Sci. U. S. A. 105, 12569–12574.
Sripada, C., Kessler, D., Fang, Y., Welsh, R.C., Kumar, K.P., Angstadt, M., 2014. Disrupted network architecture of the resting brain in attention-deficit/hyperactivity disorder. Hum. Brain Mapp. 35 (9), 4693–4705.
Supekar, K., Menon, V., Rubin, D., Musen, M., Greicius, M.D., 2008. Network analysis of intrinsic functional brain connectivity in Alzheimer's disease. PLoS Comput. Biol. 4, e1000100.
Thesen, S., Heid, O., Mueller, E., Schad, L.R., 2000. Prospective acquisition correction for head motion with image-based tracking for real-time fMRI. Magn. Reson. Med. 44, 457–465.
Vincent, J.L., Kahn, I., Snyder, A.Z., Raichle, M.E., Buckner, R.L., 2008. Evidence for a frontoparietal control system revealed by intrinsic functional connectivity. J. Neurophysiol. 100, 3328–3342.
Wang, Y., Risacher, S.L., West, J.D., McDonald, B.C., MaGee, T.R., Farlow, M.R., et al., 2013. Altered default mode network connectivity in older adults with cognitive complaints and amnestic mild cognitive impairment. J. Alzheimers Dis. 35 (4), 751–760.
Wechsler, D., 1987. Wechsler Memory Scale-Revised Manual. The Psychological Corporation, San Antonio, TX.
Wechsler, D., 1997. Wechsler Adult Intelligence Scale–Third Edition and Wechsler memory Scale–Third Edition technical manual. The Psychological Corporation, San Antonio, TX.
Weiler, M., Teixeira, C.V.L., Nogueira, M.H., Machado de Campos, B., Damasceno, B.P., Cendes, F., Balthazar, M.L.F., 2014. Differences and the relationship in default mode network intrinsic activity and functional connectivity in mild alzheimer's disease and amnestic mild cognitive impairment. Brain Connect 4 (8), 567–574.
Weintraub, S., Salmon, D., Mercaldo, N., Ferris, S., Graff-Radford, N.R., Chui, H., et al., 2009. The Alzheimer's disease centers' uniform data set (UDS): the neuropsychological test battery. Alzheimer Dis. Assoc. Disord. 23, 91–101.
Weintraub, S., Besser, L., Dodge, H.H., Teylan, M., Ferris, S., Goldstein, F.C., et al., 2018. Version 3 of the alzheimer disease centers' neuropsychological test battery in the uniform data set (UDS). Alzheimer Dis. Assoc. Disord. 32, 10–17.
Weissman, D.H., Roberts, K.C., Visscher, K.M., Woldorff, M.G., 2006. The neural bases of momentary lapses in attention. Nat. Neurosci. 9, 971–978.
Whitfield-Gabrieli, S., Ford, J.M., 2012. Default mode network activity and connectivity in psychopathology. Annu. Rev. Clin. Psychol. 8, 49–76.
Wig, G.S., 2017. Segregated systems of human brain networks. Trends Cogn. Sci. 21, 981–996.
Xu, J., Moeller, S., Auerbach, E.J., Strupp, J., Smith, S.M., Feinberg, D.A., et al., 2013. Evaluation of slice accelerations using multiband echo planar imaging at 3 T. NeuroImage 83, 991–1001.
Yeo, B.T.T., Krienen, F.M., Sepulcre, J., Sabuncu, M.R., Lashkari, D., Hollinshead, M., et al., 2011. The organization of the human cerebral cortex estimated by intrinsic functional connectivity. J. Neurophysiol. 106 (3), 1125–1165.
Zalesky, A., Fornito, A., Bullmore, E.T., 2010. Network-based statistic: identifying differences in brain networks. NeuroImage 53 (4), 1197–1207.
Zhu, D.C., Majumdar, S., Korolev, I.O., Berger, K.L., Bozokia, A.C., 2013. Alzheimer's disease and amnestic mild cognitive impairment weaken connections within the default-mode network: a multi-modal imaging study. J. Alzheimers Dis. 34, 969–984.